Phase diagram and magnetic collective excitations of the Hubbard model for graphene sheets and layers

N. M. R. Peres,[1,2] M. A. N. Araújo,[2,3] and Daniel Bozi[1,2]
[1]*Departamento de Física, Universidade do Minho, P-4710-057, Braga, Portugal*
[2]*GCEP-Center of Physics, Universidade do Minho, P-4710-057, Braga, Portugal*
[3]*Departamento de Física, Universidade de Évora, P-7000, Évora, Portugal*
(Received 15 March 2004; revised manuscript received 12 May 2004; published 29 November 2004)

We discuss the magnetic phases of the Hubbard model for the honeycomb lattice both in two and three spatial dimensions. A ground state phase diagram is obtained depending on the interaction strength U and electronic density n. We find a first order phase transition between ferromagnetic regions where the spin is maximally polarized (Nagaoka ferromagnetism) and regions with smaller magnetization (weak ferromagnetism). When taking into account the possibility of spiral states, we find that the lowest critical U is obtained for an ordering momentum different from zero. The evolution of the ordering momentum with doping is discussed. The magnetic excitations (spin waves) in the antiferromagnetic insulating phase are calculated from the random-phase approximation for the spin susceptibility. We also compute the spin fluctuation correction to the mean field magnetization by virtual emission/absorption of spin waves. In the large U limit, the renormalized magnetization agrees qualitatively with the Holstein-Primakoff theory of the Heisenberg antiferromagnet, although the latter approach produces a larger renormalization.

DOI: 10.1103/PhysRevB.70.195122 PACS number(s): 71.10.Fd, 75.10.Lp, 75.30.Ds, 75.30.Kz

I. INTRODUCTION

The interest in strongly correlated systems in frustrated lattices has increased recently because of the possible realization of exotic magnetic states,[1] spin and charge separation in two dimensions,[2] and the discovery of superconductivity in $Na_xCoO_2 \cdot yH_2O$.[3] Many researchers have discussed superconductivity in non-Bravais lattices, mainly using self-consistent spin fluctuation approaches to the problem.[4–6] The honeycomb lattice, which is made of two interpenetrating triangular lattices, has received special attention after the discovery of superconductivity in MgB_2.[7] Additionally, the honeycomb lattice has been shown to stage many different types of exotic physical behaviors in magnetism and the growing experimental evidence of non-Fermi liquid behavior in graphite has led to the study of electron-electron correlations and quasiparticle lifetimes in graphite.[8]

Around a decade ago, Sorella and Tossatti[9] found that the Hubbard model in the half-filled honeycomb lattice would exhibit a Mott-Hubbard transition at finite U. Their Monte Carlo results were confirmed by variational approaches and reproduced by other authors.[10,11] As important as the existence of the Mott-Hubbard transition in strongly correlated electron systems is the possible realization of Nagaoka ferromagnetism. The triangular, the honeycomb, and the Kagomé lattices were studied, but a strong tendency for a Nagaoka type ground state was found only in nonbipartite lattices (triangular and Kagome).[12] On the other hand, the effect of *long range* interactions in half-filled sheets of graphite was considered from a mean field point of view, using an extended Hubbard model. A large region of the phase diagram having a charge density wave ground state was found.[13] More recently, the existence of a magnetic excitation in paramagnetic graphite has been claimed,[14] but its existence was reanalyzed by two of the present authors.[15]

In this work the magnetic phases of the Hubbard model in the honeycomb lattice are studied. In addition to the two-dimensional problem we also address the three-dimensional system composed of stacked layers. The critical lines associated with instabilities of the paramagnetic phase are obtained in the U,n plane (interaction versus particle density). Spiral spin phases are also considered. A ground state phase diagram containing ferro and antiferromagnetic order is obtained. Interestingly, we find ferromagnetic regions with fully polarized spin in the vicinity of regions with smaller magnetization.

We also address the calculation of the magnetic excitations (spin waves) in the half-filled antiferromagnetic honeycomb layer within the random-phase approximation (RPA). It is known that the Hartree-Fock-RPA theory of the half-filled Hubbard model is correct in both weak and strongly interacting limits: at strong coupling, the spin wave dispersion obtained in RPA agrees with the Holstein-Primakoff theory for the Heisenberg model; at intermediate interactions ($U/t \sim 6$), the RPA dispersion shows excellent agreement with experiment.[16,17] The Hartree-Fock-RPA theory should, therefore, be considered as a useful starting point to study the intermediate coupling regime. Starting from the spin wave spectrum obtained in RPA theory, we calculate the quantum fluctuation correction to the ground state magnetization arising from virtual emission/reabsorption of spin waves. In the strong coupling limit, we find a ground state magnetization which is about 67% of full polarization. This is not so great a reduction as predicted by the Holstein-Primakoff theory of the Heisenberg model, which is about 48%.

Our paper is organized as follows: in Sec. II we introduce the Hamiltonian and its mean field treatment. In Sec. III, we discuss the possibility of a well defined magnetic excitation in the paramagnetic phase. In the ordered phase at half filling, the spin wave spectrum is computed and the effect of

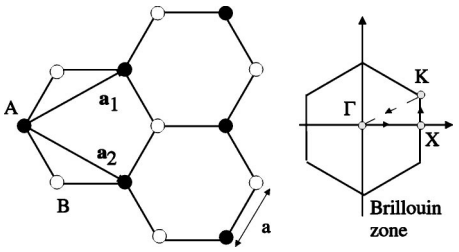

FIG. 1. Primitive vectors for the honeycomb lattice and the corresponding Brillouin zone.

different hopping terms in the spin wave spectrum is discussed. In Sec. IV, the magnetic instability lines are obtained and the possibility of spiral spin phases for $n<1$ is discussed. The corresponding lowest critical U is determined as function of the ordering wave vector $\mathbf{q}$. Section V is devoted to the phase diagram of the system, where two different types of ferromagnetism are found. The first order critical lines separating the three ordered phases are determined. Section VI contains a study of the renormalization of the electron's spectral function and magnetization by the spin wave excitations.

II. MODEL HAMILTONIAN

The magnetic properties of the honeycomb lattice is discussed in the context of the Hubbard model, which is defined as

$$\hat{H} = -\sum_{i,j,\sigma} t_{i,j}\hat{c}^{\dagger}_{i,\sigma}\hat{c}_{j,\sigma} + U\sum_{i}\hat{c}^{\dagger}_{i,\uparrow}\hat{c}_{i,\uparrow}\hat{c}^{\dagger}_{i,\downarrow}\hat{c}_{i,\downarrow} - \mu\sum_{i,\sigma}\hat{c}^{\dagger}_{i,\sigma}\hat{c}_{i,\sigma}, \tag{1}$$

where $t_{i,j}$ are hopping integrals, U is the onsite repulsion, and μ denotes the chemical potential. The honeycomb lattice is not a Bravais lattice since there are two atoms per unit cell. Therefore, it is convenient to define two sublattices, A and B, as shown in Fig. 1.

The expressions for the lattice vectors are

$$\mathbf{a_1} = \frac{a}{2}(3,\sqrt{3},0), \quad \mathbf{a_2} = \frac{a}{2}(3,-\sqrt{3},0), \quad \mathbf{a_3} = c(0,0,1), \tag{2}$$

where a is the length of the hexagon side and c is the interlayer distance. The reciprocal lattice vectors are given by

$$\mathbf{b}_1 = \frac{2\pi}{3a}(1,\sqrt{3},0), \quad \mathbf{b}_2 = \frac{2\pi}{3a}(1,-\sqrt{3},0), \quad \mathbf{b}_3 = \frac{2\pi}{c}(0,0,1). \tag{3}$$

The nearest neighbors of an atom belonging to the A sublattice are

$$\delta_1 = \frac{a}{2}(1,\sqrt{3},0) \quad \delta_2 = \frac{a}{2}(1,-\sqrt{3},0) \quad \delta_3 = -a\hat{\mathbf{x}}, \quad \delta'' = \pm c\hat{\mathbf{z}}, \tag{4}$$

while the second nearest neighbors (in the plane) are: $\delta'_1 = \pm\mathbf{a}_1, \delta'_2 = \pm\mathbf{a}_2, \delta'_3 = \pm(\mathbf{a}_2 - \mathbf{a}_1)$. In a broken symmetry state, antiferromagnetic (AF) order is described by the average lattice site occupation

$$\langle\hat{n}_{j,\sigma}\rangle = \frac{n}{2} \pm \frac{m}{2}\sigma\cos(cQ_z)\begin{cases} +, j \in A \\ -, j \in B \end{cases}, \tag{5}$$

where the z-axis ordering vector $\mathbf{Q}=(0,0,Q_z)$ will be used when studying multilayers, n denotes the electron density, m is the staggered magnetization, and $\sigma=\pm 1$. We introduce field operators for each sublattice satisfying the usual Fourier transformations

$$\hat{a}^{\dagger}_{i\in A,\sigma} = \frac{1}{\sqrt{N}}\sum_{\mathbf{k}} e^{i\mathbf{k}\cdot\mathbf{R}_i}\hat{a}^{\dagger}_{\mathbf{k}\sigma}, \quad \hat{b}^{\dagger}_{i\in B,\sigma} = \frac{1}{\sqrt{N}}\sum_{k} e^{i\mathbf{k}\cdot\mathbf{R}_i}\hat{b}^{\dagger}_{\mathbf{k}\sigma}, \tag{6}$$

where N denotes the number of unit cells. Within a Hartree-Fock decoupling of the Hubbard interaction in Eq. (1) we obtain an effective Hamiltonian matrix

$$\hat{H} = \sum_{\mathbf{k}\sigma}[\hat{a}^{\dagger}_{\mathbf{k}\sigma}\hat{b}^{\dagger}_{\mathbf{k}\sigma}]\begin{bmatrix} H_{11} & H_{12} \\ H_{21} & H_{22} \end{bmatrix}\begin{bmatrix} \hat{a}_{\mathbf{k}\sigma} \\ \hat{b}_{\mathbf{k}\sigma} \end{bmatrix}, \tag{7}$$

with matrix elements given by

$$H_{11} = D(\boldsymbol{k}) + U\frac{n-\sigma m}{2}, \quad H_{12} = \phi_{\mathbf{k}} = H^{*}_{21},$$

$$H_{22} = D(\mathbf{k}) + U\frac{n+\sigma m}{2}, \tag{8}$$

where

$$\phi_{\mathbf{k}} = -t\sum_{\delta} e^{i\mathbf{k}\cdot\delta}, \quad D(\mathbf{k}) = \phi'_{\mathbf{k}} - 2t''\cos(ck_z) - \mu,$$

$$\phi'_{\mathbf{k}} = -t'\sum_{\delta'} e^{ik\cdot\delta'}. \tag{9}$$

In Eqs. (8) and (9) t and t' are the first and second neighbor hopping integrals, respectively, while t'' describes interlayer hopping. The dispersion relation for the case where $t'=t''=0$ and $U=0$ is

$$|\phi_k| = \pm t\sqrt{3 + 2\cos(\sqrt{3}ak_y) + 4\cos(3ak_x/2)\cos(\sqrt{3}ak_y/2)}. \tag{10}$$

Diagonalization of the effective Hamiltonian yields a two band spectrum. The band energies are:

$$E_{\pm}(\boldsymbol{k}) = D(\boldsymbol{k}) + \frac{U}{2}n \pm \sqrt{\left(\frac{Um}{2}\right)^2 + |\phi_k|^2}. \tag{11}$$

Because there are two sublattices, the Matsubara Green's function is a 2×2 matrix whose elements are given by

$$\mathcal{G}^{aa}_{\sigma}(i\omega,\boldsymbol{k}) = \sum_{j=\pm}\frac{|A_{\sigma,j}|^2}{i\omega - E_j(\boldsymbol{k})}, \tag{12}$$

$$\mathcal{G}^{ab}_{\sigma}(i\omega,\boldsymbol{k}) = \sum_{j=\pm}\frac{A_{\sigma,j}B^{*}_{\sigma,j}}{i\omega - E_j(\boldsymbol{k})}, \tag{13}$$

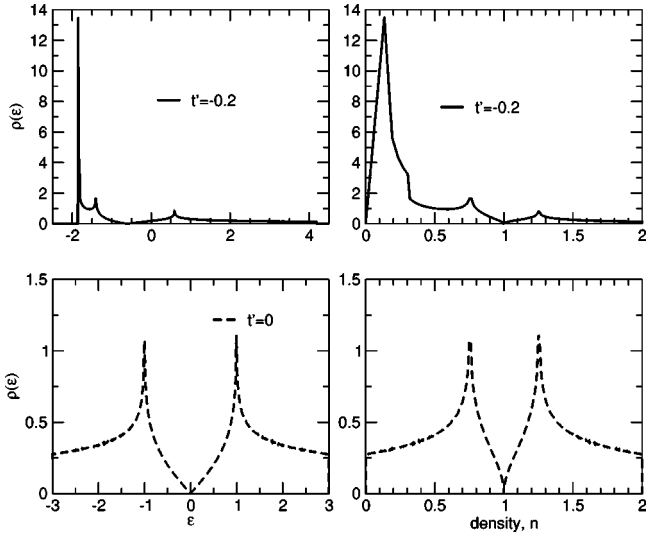

FIG. 2. Single particle density of states, $\rho(\epsilon)$, for independent electrons in an honeycomb lattice. The left and right panels show $\rho(\epsilon)$ as function of energy and electron density, respectively. The solid line refers to $t'=-0.2$ and the dashed line to $t'=0$.

$$\mathcal{G}_{\sigma}^{ba}(i\omega,\boldsymbol{k})=\sum_{j=\pm}\frac{A_{\sigma,j}^{*}B_{\sigma,j}}{i\omega-E_{j}(\boldsymbol{k})}, \tag{14}$$

$$\mathcal{G}_{\sigma}^{bb}(i\omega,\boldsymbol{k})=\sum_{j=\pm}\frac{|B_{\sigma,j}|^{2}}{i\omega-E_{j}(\boldsymbol{k})}, \tag{15}$$

where the coherence factors are

$$|A_{\sigma,\pm}(\boldsymbol{k})|^{2}=\frac{1}{2}\left[1-\frac{Um\sigma}{2E_{\pm}(\boldsymbol{k})}\right],$$

$$|B_{\sigma,\pm}(\boldsymbol{k})|^{2}=\frac{1}{2}\left[1+\frac{Um\sigma}{2E_{\pm}(\boldsymbol{k})}\right], \tag{16}$$

$$A_{\sigma,\pm}(\boldsymbol{k})B_{\sigma,\pm}^{*}(\boldsymbol{k})=-\frac{\phi(\boldsymbol{k})}{2E_{\pm}(\boldsymbol{k})}. \tag{17}$$

In the ferromagnetic (F) phase, the site occupation is the same for both sublattices

$$\langle\hat{n}_{j,\sigma}\rangle=\frac{n}{2}+\frac{m}{2}\sigma,\quad j\in A,B. \tag{18}$$

In this case the quasiparticle energy bands are given by

$$E_{\pm}^{\sigma}(\boldsymbol{k})=D(\boldsymbol{k})+\frac{U}{2}(n-\sigma m)\pm|\phi_{\mathbf{k}}|. \tag{19}$$

In the paramagnetic phase of the system the energies and propagators are simply obtained by setting $m=0$ in the equations above. The density of states of single electrons is shown in Fig. 2 against particle density and energy. In the two upper panels we have included a second-neighbor hopping while in the two lower panels only nearest neighbor coupling is considered. An important feature is that $\rho(\epsilon)$ vanishes linearly with ϵ as we approach the half filled limit, both for $t'=0$ and $t'\neq 0$. This is related to the K points of the Brillouin Zone (see Fig. 1), where the electron dispersion becomes linear

$$E(\boldsymbol{k})\approx\pm t\frac{3a}{2}|d\boldsymbol{k}|,$$

$d\boldsymbol{k}$ denotes the deviation from the K point. This dispersion is called the "Dirac cone."

III. COLLECTIVE EXCITATIONS AT HALF FILLING

The magnetic excitations are obtained from the poles of the transverse spin susceptibility tensor, χ, which is defined, in Matsubara form, as

$$\chi_{+-}^{i,j}(\boldsymbol{q},i\omega_{n})=\int_{0}^{1/T}d\tau\, e^{i\omega_{n}\tau}\langle T_{\tau}\hat{S}_{i}^{+}(\boldsymbol{q},\tau)\hat{S}_{j}^{-}(-\boldsymbol{q},0)\rangle, \tag{20}$$

where $i,j=a,b$ label the two sublattices (not lattice points) and $S_{i}^{+}(\boldsymbol{q}),S_{j}^{-}(\boldsymbol{q})$ denote the spin raising and lowering operators for each sublattice.

In the paramagnetic, F, or AF phases, the zero order susceptibility is just a simple bubble diagram with the Green's functions given in Eqs. (12)–(15):

$$\chi_{+-}^{(0)i,j}(\boldsymbol{q},i\omega_{n})=-\frac{T}{N}\sum_{k,\omega_{m}}\mathcal{G}_{\uparrow}^{ji}(\boldsymbol{k},i\omega_{n})\mathcal{G}_{\downarrow}^{ij}(\boldsymbol{k}-\boldsymbol{q},i\omega_{n}-i\omega_{m}). \tag{21}$$

Going beyond mean-field, the RPA result for the susceptibility tensor is obtained from the Dyson equation

$$\chi=\chi^{0}+U\chi^{0}\chi\Rightarrow\chi=[\hat{I}-U\chi^{0}]^{-1}\chi^{0}, \tag{22}$$

where $\hat{I}$ denotes the 2×2 identity matrix. The poles of the susceptibility tensor, corresponding to the magnetic excitations, are then obtained from the condition

$$\mathrm{Det}[\hat{I}-U\chi^{0}]=0. \tag{23}$$

We note that the tensorial nature of the spin susceptibility is a consequence of there being two sites per unit cell and is not related to the magnetic order in the system.

A. Magnetic excitations in a single paramagnetic layer

Here we discuss the possibility of existence of magnetic excitations in a single honeycomb paramagnetic layer. Our interest in this problem stems from a recent claim, by Baskaran and Jafari,[14] who recently proposed the existence of a neutral spin collective mode in graphene sheets. In the calculations of Ref. 14 a half-filled Hubbard model in the honeycomb lattice (with $t'=t''=0$) was considered but the tensorial character of the susceptibility was neglected.[15] Since inelastic neutron scattering can be used to study this spin collective mode in graphite, we decided to re-examine this problem taking into account the tensorial nature of the transverse spin susceptibility.

Collective magnetic modes with frequency ω and momentum $\boldsymbol{q}$ are determined from the condition (23) after perform-

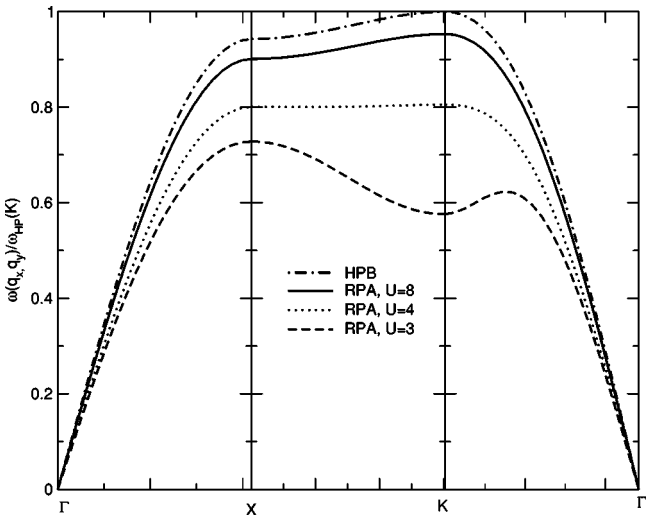

FIG. 3. Spin-wave excitation spectrum for several values of U. The dashed-dotted line gives the Holstein-Primakoff result for the Heisenberg antiferromagnet in the honeycomb lattice.

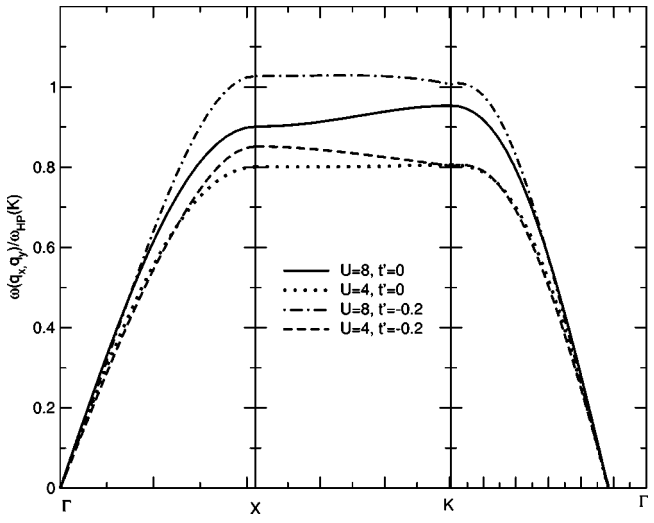

FIG. 4. Spin-wave excitation spectrum for several values of U and $t' \neq 0$.

ing the analytic continuation $i\omega \rightarrow \omega + i0^+$. The determinant is given by

$$D_{+-}(\boldsymbol{q},\omega) = 1 - 2U\chi^{(0)aa}_{+-} + U^2[(\chi^{(0)aa}_{+-})^2 - \chi^{(0)ab}_{+-}\chi^{(0)ba}_{+-}], \tag{24}$$

where we have taken into account that in a paramagnetic system $\chi^{(0)aa}_{+-} = \chi^{(0)bb}_{+-}$. Below the particle-hole continuum of excitations, the spectral (delta-function contributions) part in $\chi^{(0)ij}_{+-}(\boldsymbol{q},\omega+i0^+)$ vanishes and there is the additional relation $\chi^{(0)ba}_{+-} = [\chi^{(0)ab}_{+-}]^*$.Collective modes are only well defined outside the particle-hole continuum (inside the continuum they become Landau damped). We searched[15] for well defined magnetic modes, $\omega(\boldsymbol{q})$, below the continuum of particle-hole excitations, and found no solutions for any value of the interaction U. In Fig. 1 of Ref. 15 we plot $D_{+-}(\boldsymbol{q},\omega)$ for eight different $\boldsymbol{q}$ vectors and ω ranging from zero to the point where the particle hole continuum begins. Our analysis reveals that the full tensorial structure of the Hubbard model's RPA susceptibility in the honeycomb lattice does not predict a collective magnetic mode.

B. Spin waves in the antiferromagnetic layer

The spin wave dispersion $\omega(\boldsymbol{q})$ for the AF layer with one electron per site can be obtained from Eqs. (21) and (23) using expressions (12)–(15) for the propagators. Spin wave spectra, for different values of second-neighbor hopping, t', are plotted in Figs. 3 and 4. In the large U limit, spin wave energies agree with those obtained from the Holstein-Primakoff theory of the Heisenberg model. We give an analytical derivation of this limit in Appendix B. The Holstein-Primakoff result for the Heisenberg model in the honeycomb lattice, which is derived in Appendix C, can be written as

$$\omega_{\mathrm{HP}}(\boldsymbol{q}) = JS\sqrt{z^2 - |\phi(\boldsymbol{q})|^2}. \tag{25}$$

This result can be mapped on the Hubbard model provided that $J = 4t^2/U$ and $S = 1/2$. Figure 3 shows the spin wave energies for the two-dimensional (2D) lattice ($t' = 0$) along a closed path in the Brillouin Zone. Energies in Fig. 3 are normalized by the Holstein-Primakov result at the K point, $\omega_{\mathrm{HP}}(K)$ (see Fig. 1). It can be seen that the results for $U = 8$ are very close to the asymptotic behavior of the RPA, whereas, for smaller U, the spin wave energy is reduced. The effect of t' on $\omega(\boldsymbol{q})$ is depicted in Fig. 4. It is of particular interest the fact that the dispersion along the X-K direction is almost absent for $U \geqslant 4$. The presence of t' does not change this effect.

IV. MAGNETIC INSTABILITIES

The magnetic instabilities in the paramagnetic phase can be obtained from the divergence of the RPA susceptibilities at critical values of the interaction, U_c, driving the system towards a magnetically ordered phase. At a given electron density n we always find two instability solutions, one ferromagnetic and one antiferromagnetic. One of these solutions minimizes the free energy. Since U_c is determined from $D_{+-}(\boldsymbol{q},0) = 0$, taking into account that $\chi^{(0)aa}_{+-} = \chi^{(0)bb}_{+-}$ and $\chi^{(0)ab}_{+-} = (\chi^{(0)ba}_{+-})^*$ in the paramagnetic phase, we obtain

$$U_c = \frac{1}{\chi^{(0)aa}_{+-} \pm |\chi^{(0)ab}_{+-}|}. \tag{26}$$

Figure 5 shows U_c obtained from the static uniform susceptibilities ($\boldsymbol{q} = \boldsymbol{0}$ and $\omega = 0$), as a function of electron density for various values of t'. Detailed equations for the instability lines are given in Appendix A. The left panel of Fig. 5 refers to the 2D case, corresponding to a single honeycomb layer, whereas the right panel refers to the three-dimensional (3D) system with a constant interlayer hopping $t'' = 0.1$. The Van Hove singularity (associated with the X point) plays an important role.

As we have already mentioned, the two solutions of Eq. (26) correspond to two different magnetic transitions, one between a paramagnetic phase and a ferromagnetic phase

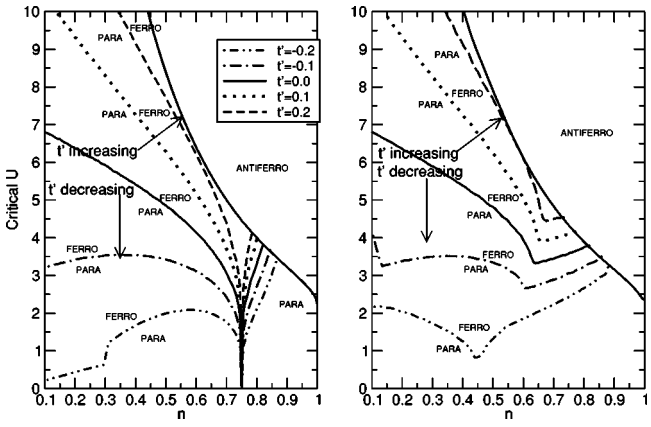

FIG. 5. Left panel: Effect of t' on the instability lines, as determined from Eq. (26) , for a single honeycomb layer. Right panel: Effect of t' on the instability lines, as determined from Eq. (26) , for a layered honeycomb. This panel differs from the other inasmuch a small $t''=0.1$ hoping term was included coupling the 2D layers.

and another between a paramagnetic phase and an antiferromagnetic phase. That this is so can easily be confirmed by solving the self-consistent equations for the ferromagnetic and the antiferromagnetic magnetizations, respectively, derived from the HF Hamiltonian (7). By minimizing the free energy with respect to magnetization, one finds the following expressions for ferro- and antiferromagnetic magnetizations:

$$m_F = \frac{1}{2N}\sum_{k\sigma} \sigma[f(E_+^\sigma) + f(E_-^\sigma)],$$

$$m_{\mathrm{AF}} = \frac{1}{N}\sum_{\mathbf{k}} \frac{|\zeta_{\mathbf{k}}|}{\sqrt{1+\zeta_{\mathbf{k}}^2}}[f(E_-) - f(E_+)], \qquad (27)$$

where $f(x)$ is the Fermi function and $\zeta_{\mathbf{k}} = Um_{\mathrm{AF}}/(2|\phi_{\mathbf{k}}|)$. Letting both m_F and m_{AF} approach zero, one obtains the same lines as those in Fig. 5. Generally speaking, for electron densities lower than 0.85, the value of U_c that separates the paramagnetic region from the ferromagnetic region is lower than the corresponding value of U_c separating the paramagnetic region from the antiferromagnetic region. The critical U associated with the ferromagnetic instability increases with t'. The size of the paramagnetic region in Fig. 5 increases with t'. On the other hand, for $t'=0.2$, we see that the critical line for the ferromagnetic region is very close to the critical line of the antiferromagnetic region. Therefore, the ferromagnetic region is progressively shrinking with increasing t'. If we now turn to densities larger than 0.85, we find that the antiferromagnetic critical line is the one with lowest U_c. However, in contrast to lower densities, the antiferromagnetic critical line hardly changes when varying t'. This description applies equally well to the single honeycomb layer and weakly coupled layers, even though the quantitative functional dependence of U_c on n is different in the two cases, the main difference coming from the van Hove singularity present in the 2D case. At finite temperature the van Hove singularity is rounded off and the 2D phase diagram will be much more similar to the 3D case. We therefore, consider that a weak 3D interlayer coupling does not qualitatively modify the conclusions valid for the 2D case.

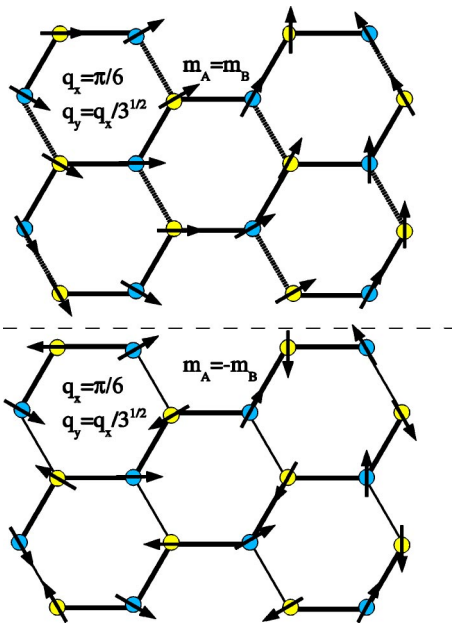

FIG. 6. (Color online) F_q (upper) and AF_q (lower) spin configurations for $q_x=\pi/6$.

Besides collinear spin phases, the system may also present noncollinear spiral spin phases in some regions of the phase diagram. We now study what are the changes in the critical U values determining the instability of the paramagnetic phase if we allow for noncollinear ground states, since it is well known that the Hubbard model on bipartite and non-bipartite lattices can have the lowest U_c for spiral spin phases[12,18,19] for some electronic densities. In a spiral state, the spin expectation value at site i, belonging to sublattice $\nu=a,b$, is given by[20]

$$\langle \boldsymbol{S}_i^\nu \rangle = \frac{m_\nu}{2}[\cos(\boldsymbol{q}\cdot\boldsymbol{R}_i^\nu), \sin(\boldsymbol{q}\cdot\boldsymbol{R}_i^\nu)]. \qquad (28)$$

If $\boldsymbol{q}\neq\mathbf{0}$, the ferromagnetic and antiferromagnetic spin configurations become twisted. We shall refer to the twisted $\boldsymbol{q}\neq\mathbf{0}$ configurations as "F_q" whenever $m_A=m_B$, and "AF_q" whenever $m_A=-m_B$. The criterion for choosing the $\mathbf{q}$ vectors is taken directly from the geometry of the lattice by requesting a constant angle between spins on neighboring sites, i.e., $\boldsymbol{q}\cdot\boldsymbol{\delta}_1=\boldsymbol{q}\cdot\boldsymbol{\delta}_2=-\boldsymbol{q}\cdot\boldsymbol{\delta}_3$. Unfortunately, however, this cannot be achieved in the honeycomb lattice with only one $\boldsymbol{q}$ vector. The closest one can get to a "true" spiraling state is by letting $\boldsymbol{q}\cdot\boldsymbol{\delta}_1=-\boldsymbol{q}\cdot\boldsymbol{\delta}_3$ (or equivalently, $\boldsymbol{q}\cdot\boldsymbol{\delta}_2=-\boldsymbol{q}\cdot\boldsymbol{\delta}_3$), which implies that $\boldsymbol{q}=(q_x,q_y)=q_x(1,1/\sqrt{3})$ $[\boldsymbol{q}=q_x(1,-1/\sqrt{3})]$. For the moment we let q_z be zero which means that we consider identical layers. The condition $\boldsymbol{q}\cdot\boldsymbol{\delta}_1=-\boldsymbol{q}\cdot\boldsymbol{\delta}_3$ means that the increase in spin angle between two lattice sites in the $-\boldsymbol{\delta}_3$ direction is the same as the increase in spin angle between two lattice sites in the $\boldsymbol{\delta}_1$ direction. There is no increase in the spin angle in the $\boldsymbol{\delta}_2$ direction. Examples of the spin configurations obtained in this way are shown in Figs. 6 and 7. Several notes are in order at this stage. First, although we do not have a true spiraling state over the whole lattice, we do

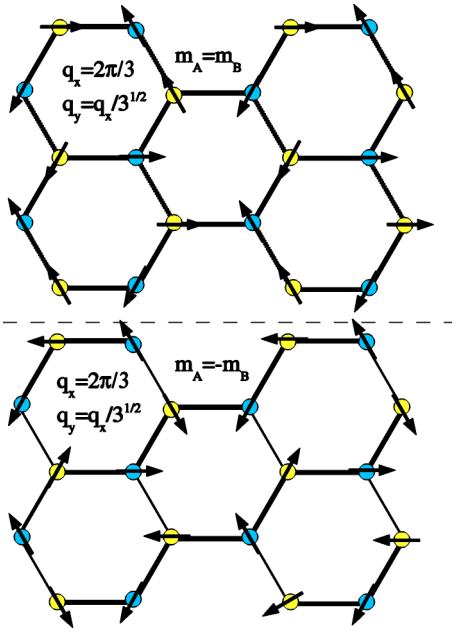

FIG. 7. (Color online) F_q (upper) and AF_q (lower) spin configurations for $q_x=2\pi/3$.

have a spiraling configuration in the $-\boldsymbol{\delta}_3$ and $\boldsymbol{\delta}_1$ directions, as can be seen from the Figs. 6 and 7, going from the lower left to upper right. Second, when traveling along the $\boldsymbol{\delta}_2$ direction, the spin angles do not increase. Instead, neighboring spins in this direction are always aligned ferromagnetically when $m_A=m_B$, and antiferromagnetically when $m_A=-m_B$. However, two successive $\boldsymbol{\delta}_2$ bonds ("sliding down" the lattice from left to right) have the same increase in spin angle as any two neighbors connected by $-\boldsymbol{\delta}_3$ or $\boldsymbol{\delta}_1$. The $\boldsymbol{q}$ vector (i.e., the spin configuration) that a system with a given density would prefer is the one with the lowest value of $U_c(\boldsymbol{q})$. In Fig. 8 we present a curve showing the $\boldsymbol{q}$ vectors that minimize $U_c(\boldsymbol{q})$, as functions of particle density n. We consider discrete values $q_x=i(\pi/12)$ with $i=0,1,\ldots,12$. The dependence on t' is overall the same as that discussed for $\boldsymbol{q}=\boldsymbol{0}$ (for example, the shrinking effect with increasing t' is also seen here). There is no reason to restrict $\boldsymbol{q}$ to integer multiples of $\pi/12$, other than a pure computational one. By performing the same calculation with more $\boldsymbol{q}$ vectors, the "step function" like appearance of the lower graphs of Fig. 8 can be smoothed out. Our analysis is sufficient, however, to get an insight into how the $\boldsymbol{q}$ vectors (which minimize U_c) vary with n.

The solid line limiting the paramagnetic region is shown in the lower graphs of Fig. 8. We see that the behavior of q_x, as function of n, is almost the same for the 2D and 3D cases. As the system approaches half filling, the preferred spin configuration approaches that with $\boldsymbol{q}=\boldsymbol{0}$. In a doped system, however, minimization of $U_c(\boldsymbol{q})$ is attained for a nonzero $\boldsymbol{q}$. It is also seen that the dependence of $\boldsymbol{q}$ on n is not monotonic. Either in 2D or 3D, q_x goes all the way from 0 (at $n=1$) to π, displaying two local maxima (and a local minimum in between) as n ranges from 1 towards 0.

The value of q_x reaches a local minimum at $q_x=7\pi/12$, at $n=0.37$ (in 2D) or at $n=0.45$ (in 3D). For even lower densities, q_x attains another maximum at $q_x=\pi$, which means that the spins of any two nearest neighbors, in the $-\boldsymbol{\delta}_3$ and $\boldsymbol{\delta}_1$ directions, point exactly in opposite directions to each other.

The same type of behavior is seen also for the critical line separating magnetically ordered phases (dashed line). Again, the 2D and the 3D cases are very similar to each other. For densities around 0.30–0.35 (2D) and 0.35–0.40 (3D), we have $q_x=8\pi/12$ yielding the lowest U_c. Moreover, the solid and the dashed lines coincide, illustrating the previously mentioned ferromagnetic "shrinking out" effect. In other words, for $q_x=8\pi/12$, the two solutions of $U_c(\boldsymbol{q})$ almost coincide for all n, leaving only a thin strip of ferromagnetism

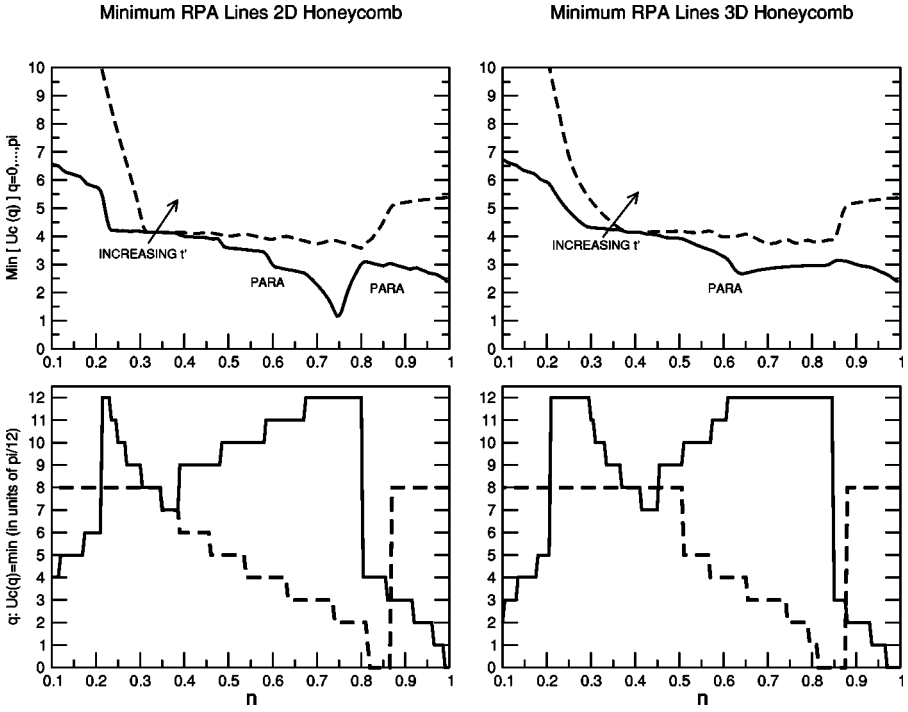

FIG. 8. The upper panels show the minimum $U_c(\mathbf{q})$ according to Eq. (26) . The solid line separates the paramagnetic phase from magnetically ordered phases, while the dashed line separates differently ordered magnetic phases. The lower panels show the q_x component of the ordering vector (corresponding to the minimum U_c) as function of electron density n.

between the paramagnetic and the antiferromagnetic regions. Although this is true for all n, it is only for $n=0.37-0.40$ (2D case) and $n=0.35-0.37$ (3D case) that $U_c(q_x=8\pi/12)$ is minimum.

So far, our analysis has been restricted to $\boldsymbol{q}$ vectors lying in the x-y spin plane. This means that two interlayer neighbors have the same spin. If we now consider neighboring layers with opposite spin, we put $q_z=\pi$. At half filling, the lowest $U_c(0,0,\pi)=2.04$ limiting the paramagnetic region is lower than the corresponding $U_c(0,0,0)=2.35$, independently of t'. Moreover, for $n=1$, $U_c(q_x,q_x/\sqrt{3},\pi)$ is always lower than $U_c(q_x,q_x/\sqrt{3},0)$ for any q_x, showing that, at half filling, we should expect antiferromagnetic ordering along the z direction.

The above study was focused on the second order instability lines, both in the case of collinear and spiral spin phases, being clear that spiral states have a lower critical U value, over a large range electronic densities. It is instructive to compare our results with those of Ref. 12. Looking at Fig. 2 of Ref. 12 we see that for the triangular lattice there are some finite regions where the more stable ground states correspond to spiral states. These regions are located at electronic densities smaller than 0.5 and larger than 0.8. Since the honeycomb lattice consists of two interpenetrating triangular lattices we expect the same type of behavior, at least at the qualitative level. That is, we do expect to have finite regions of the phase diagram where spiral phases have the lowest energy. Also, in Ref. 12 the authors do not discuss the full phase diagram of the Hubbard model in the honeycomb lattice, as we do in next section. They are primarily interested in the stability of the Nagaoka state. Their study is done using three different approaches: (i) The Hartree single flip ansatz; (ii) the SKA Gutwiller ansatz; and (iii) the Basile-Elser ansatz. A comparison can be established between the Hartree single flip ansatz which roughly speaking, produces a straight line for all densities at the on-site Coulomb interaction $U\sim 5$, and our self consistent Hartree-Fock study. If we forget, for a moment, the van Hove singularity, both results are qualitatively the same for n up to 0.8. Above this value our Hartree-Fock analysis, forgetting about the existence of the antiferromagnetic phase, predicts a very strong increase of the critical U value (not shown in Fig. 5, since the AF phase presents the lowest critical U value), in agreement with the SKA ansatz. This behavior is not captured by the Hartree single flip ansatz. It seems that our study interpolates between the Hartree single flip ansatz for low densities and the SKA ansatz for densities above 0.8. Quantitatively there are differences between the two studies, which are understandable on the basis of the different types of proposed ground states.

V. PHASE DIAGRAM

As we mentioned in the previous section, the study of Ref. 12 is mainly concerned with the stability of the Nagaoka state, and in the previous section we studied the values of the Hubbard interaction associated with instabilities of the paramagnetic system. The transition from the paramagnetic to a magnetically ordered state is determined by the lowest U_c.

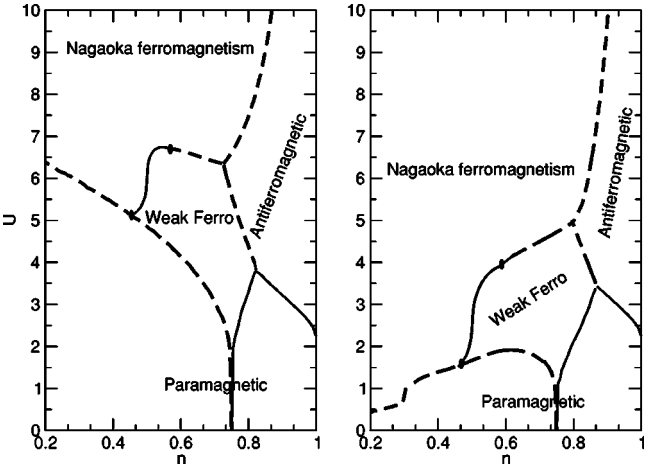

FIG. 9. **Left panel**: Ground state phase diagram of the Hubbard model in the (n,U) plane for a single layer with $t'=0$. **Right panel**: Ground state phase diagram of the Hubbard model in the (n,U) plane for a single layer with $t'=-0.2$. In both cases dashed and continuous lines represent first and second order transitions, respectively.

Since we have found the possibility of having, at least, two (ferro and antiferro) different types of ground states, then in the case where interaction is stronger than both critical values, we need to address the problem of competition between the two ordered phases. The phase with the lowest free energy is the one preferred by the system. In this section we restrict ourselves to the study of a single layer but we shall consider different band structures. Spiral states will not be considered, since we are most interested in a weak ferromagnetic phase showing up in a region of the phase diagram where the studies of Ref. 12 suggest that the collinear ferromagnetic (fully polarized) phase should be the most stable one. In the ferromagnetic phase we distinguished two types of ferromagnetic ground states: the Nagaoka ground state, with a maximally polarized spin ($m_F=n$), and a weak ferromagnetic state with $m_F<n$. The order parameter and free energies were obtained from the mean field Hamiltonian (7). Figure 9 shows the ground-state (n,U) phase diagram of the model.

The effect of t' on the phase diagram can be seen in right panel of Fig. 9. In Fig. 9 the dashed lines represent first-order phase transitions, where the order parameter do not vanish smoothly, while continuous lines represent second order transitions, where the order parameter vanishes smoothly, but its first derivative is discontinuous. In both cases ($t'=0$ and $t'\neq 0$) we find a finite region of weak ferromagnetism. In general the Nagaoka phase is more stable for large U. The weak ferromagnetic phase is separated from the Nagaoka phase by first or second order transition lines, depending on the path followed on (U,n) diagram. The second order transition manifests itself through a discontinuity of the derivative of the magnetization with respect to U. At $n=0.75$ the instability line towards the ferromagnetic phase shows a dip (pronounced if $t'=0$), which is due to the logarithmic van Hove singularity at $n=0.75$. A negative t' produces two effects on the phase diagram: (i) the instability line towards the F phase moves downwards; and (ii) the point where the instability

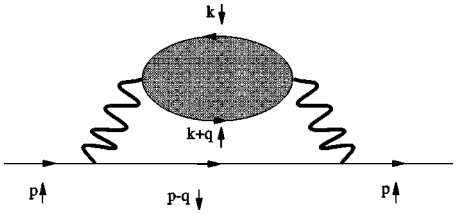

FIG. 10. The self-energy for a ↑-spin electron. The bubble represents the transverse susceptibility computed in RPA.

lines towards F and AF meet moves to larger n. Similarly to what was found in the previous section, the overall effect of t' is to modify the ferromagnetic region of the phase diagram. Further, for negative t' we expect collinear ferromagnetism to exist over a large region of the phase diagram relatively to the case $t' \geqslant 0$, since it is well known that a negative t' stabilizes the ferromagnetic phase. On the other hand we do not expect the phase diagram presented in this section to be fully accurate for low densities, where the findings of Ref. 12 should apply.

The first order critical lines do separate two different ferromagnetic (or ferromagnetic from antiferromagnetic) regions, in what concerns the total magnetization. In view of the results published in Ref. 21, where a first order transition between the two competing phases is transformed by disorder into two second order phase transitions, we expect the same behavior to apply here, that is, disorder may change the order of the transition, since the arguments put forward in Ref. 21 are of very general nature. It would be very interesting to study whether the introduction of disorder in the system could change the nature of the first order transitions.

VI. QUANTUM FLUCTUATIONS

This section is devoted to the calculation of quantum fluctuation corrections to the magnetization. An analogous calculation for the Hubbard model in the square lattice in the $t/U \to 0$ limit was sketched by Singh and Tešanović.[22,23]

The computation of the renormalized staggered magnetization requires the evaluation of the Feynman diagram shown in Fig. 10, which shows the second order (in the interaction U) contribution to the self-energy. The diagram describes the emission and later absorption of a spin wave by an up-spin electron. The emission and absorption processes are accompanied by electron spin reversal. This effect, consisting of virtual spin flips, is going to renormalize the staggered magnetization. The spin- ↑ electron Green's function is

$$\mathcal{G}_{\uparrow}(\mathbf{p}, i\omega) = \mathcal{G}^0_{\uparrow}(\mathbf{p}, i\omega) + \mathcal{G}^0_{\uparrow}(\mathbf{p}, i\omega)\Sigma_{\uparrow}(\mathbf{p}, i\omega)\mathcal{G}_{\uparrow}(\mathbf{p}, i\omega),$$

hence, $\mathcal{G}^{-1} = [\mathcal{G}^{(0)}]^{-1} - \Sigma^{-1}$. Here, $\mathcal{G}^0$ denotes the Hartree-Fock Green's functions matrix appearing in Eqs. (12)–(15). The self-energy matrix is given by

$$\Sigma^{ij}_{\uparrow}(\mathbf{p}, i\omega) = U^2 \frac{T}{N} \sum_{i\Omega, \mathbf{q}} \mathcal{G}^{(0)ij}_{\downarrow}(\mathbf{p} - \mathbf{q}, i\omega - i\Omega)\chi^{(\mathrm{RPA})ij}_{-+}(\mathbf{q}, i\Omega), \tag{29}$$

where i, j are sublattice indices. The self-energy for a ↓-spin electron would be similar to that in Eq. (29) with the $\mathcal{G}^{(0)ij}$-spin reversed and χ_{-+} replaced with χ_{+-}. The renormalized staggered magnetization at $T=0$ is given by

$$\overline{m} = -\frac{1}{N}\sum_{k\sigma} \int_{-\infty}^{0} \frac{d\omega}{2\pi} \sigma [Im\ G^{aa}_{\sigma,\mathrm{Ret}}(\boldsymbol{k}, \omega) - Im\ G^{bb}_{\sigma,\mathrm{Ret}}(\boldsymbol{k}, \omega)], \tag{30}$$

where $Im\ G^{ij}_{\sigma,\mathrm{Ret}}(\boldsymbol{k}, \omega)$ stands for the imaginary part of the retarded Green's function for a spin σ electron.

The RPA susceptibility has poles corresponding to the spin waves calculated in Sec. III, with energy $\approx |\phi(\mathbf{k})|^2/U$, but it also has poles describing a particle-hole continuum of excitations at higher energies (of order U). In what follows we ignore this particle-hole continuum and take into account only the contribution from the spin wave poles to the self-energy. Physically, this means that we shall calculate the magnetization renormalized by the spin waves. To this end, we start by replacing the susceptibility in Eq. (29) by the expression

$$\chi^{(\mathrm{RPA})ij}(\mathbf{q}, i\omega) = \frac{R^{ij}[\omega(\mathbf{q})]}{i\omega - \omega(\mathbf{q})} + \frac{R^{ij}[-\omega(\mathbf{q})]}{i\omega + \omega(\mathbf{q})}, \tag{31}$$

where $R^{ij}[\pm\omega(\mathbf{q})]$ denotes the residue of $\chi^{(\mathrm{RPA})ij}_{-+}$ at the spin wave pole with dispersion $\omega(\mathbf{q})$. Equation (31) describes an effective spin wave propagator. After performing the Matsubara frequency summation in Eq. (29) we obtain

$$\Sigma^{ij}_{\uparrow}(\mathbf{p}, i\omega) = \frac{U^2}{N}\sum_{\mathbf{q}} \left\{ \frac{\mathrm{num}[\mathcal{G}^{(0)ij}_{\downarrow,-}(\mathbf{p}-\mathbf{q})]R^{ij}[-\omega(\mathbf{q})]}{i\omega + \omega(\mathbf{q}) + E_+(\mathbf{p}-\mathbf{q})} - \frac{\mathrm{num}[\mathcal{G}^{(0)ij}_{\downarrow,+}(\mathbf{p}-\mathbf{q})]R^{ij}[\omega(\mathbf{q})]}{i\omega - \omega(\mathbf{q}) - E_+(\mathbf{p}-\mathbf{q})} \right\}, \tag{32}$$

where we have introduced the notation $\mathrm{num}\{\mathcal{G}^{(0)ij}_{\sigma,b}\}$ for the numerators of the Green's functions, as expressed in Eqs. (12)–(17).

In Figure 11 we show the renormalized magnetization versus U. The Hartree-Fock magnetization is also shown in Fig. 11 for comparison. The calculation was performed for three different lattice sizes. It can be seen that convergence does not require a very large number of $\mathbf{k}$ points in the Brillouin zone. This is not surprising because the Hartree-Fock magnetization itself already converges to the correct value in a 40×40 lattice. We have also checked that the RPA propagators return the original electron density $n=1$, meaning that no spectral weight was lost in the used approximation for the self-energy. In the large U limit, the renormalized magnetization saturates at about 67% of the (fully polarized) mean field value. This is in qualitative agreement with the Holstein-Primakoff result for the $S=1/2$ Heisenberg model in the honeycomb lattice, which predicts a ground state magnetization of 48%. We should remark, however, that the spin wave spectrum calculated within RPA theory has shown much better agreement with experimental results for Mott-Hubbard antiferromagnetic insulators than the Holstein-Primakoff theory.[16,17]

In Fig. 12 we show the imaginary part of the electron's Green's function at negative frequencies, on both sublattices, for two different values of U. It is clear that, for strong cou-

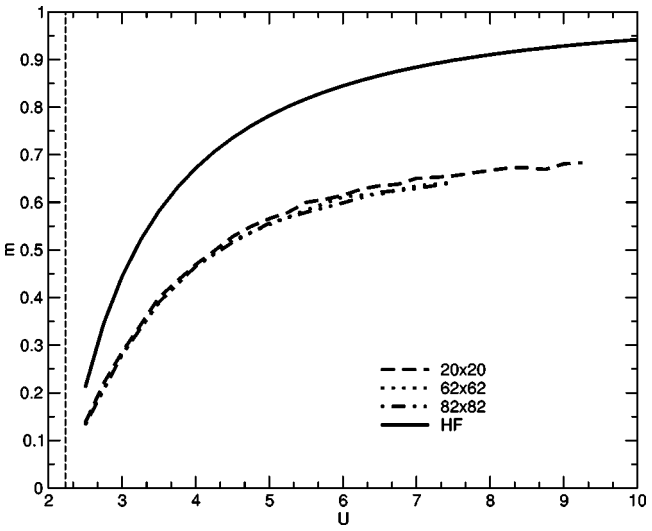

FIG. 11. The magnetization in the half-filled honeycomb AF layer. The continuous line represents the Hartree-Fock result. Renormalized magnetizations are shown for different lattice sizes:[23] 20×20; 62×62; 82×82. The vertical dashed line represents the mean field critical U value at which the magnetic instability develops.

plings, part of the Hatree-Fock spectral weight is shifted to the bottom of the (negative) energy band. This shifting of the spectral weight is responsible for the renormalization of the staggered magnetization. It is interesting to see that for low U the spectral weight is most significant at high energy, in the interval $]-2,0[$, with a much smaller weight in the interval $]-4,-2[$. At a stronger Hubbard interaction most of the high energy spectral weight (previously in the interval $]-2,0[$) has been displaced to lower energies and become localized around well defined energies, whereas the spectral weight at intermediate energy (in the interval $]-4,-2[$) remains essentially unchanged. Therefore, increasing Hubbard coupling has the effect of displacing the distribution of spectral weight from the top to the bottom of the energy band.

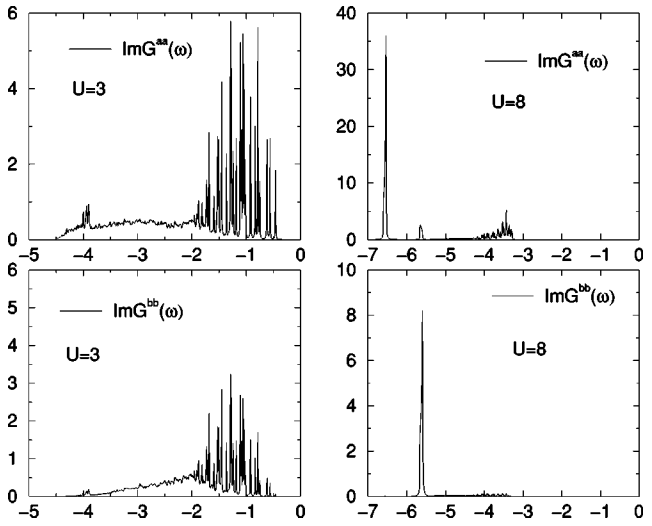

FIG. 12. Imaginary part of the retarded electron Green's function multiplied by -1, $-ImG_{\uparrow}^{aa(bb)}(\omega)$, vs negative frequency. The Green's function includes the quantum fluctuations.

Finally, a comment regarding approximation (31). The commutation relation between the spin raising and lowering operators

$$\sum_{\mathbf{p},\mathbf{p}'}[\hat{a}^{\dagger}_{\mathbf{p},\downarrow}\hat{a}_{\mathbf{p}+\mathbf{q},\uparrow},\hat{a}^{\dagger}_{\mathbf{p}'+\mathbf{q},\uparrow}\hat{a}_{\mathbf{p}',\downarrow}]=\sum_{\mathbf{p}}(\hat{a}^{\dagger}_{\mathbf{p},\downarrow}\hat{a}_{\mathbf{p},\downarrow}-\hat{a}^{\dagger}_{\mathbf{p},\uparrow}\hat{a}_{\mathbf{p},\uparrow}),$$

is equivalent to the following relation between the Hartree-Fock magnetization, m, and the transverse susceptibilities:

$$\chi^{aa}_{-+}(\mathbf{q},\tau=0^{+})-\chi^{aa}_{-+}(\mathbf{q},\tau=0^{-})=\oint_{-i\infty}^{+i\infty}\frac{-idz}{2\pi}\chi^{aa}_{-+}(z)e^{-z0^{+}}$$

$$-\oint_{-i\infty}^{+i\infty}\frac{-idz}{2\pi}\chi^{aa}_{-+}(z)e^{z0^{+}}=-m, \tag{33}$$

at $T=0$. The integration of the term $e^{-z0^{+}}$ ($e^{z0^{+}}$) is performed along the semicircular contour on the right (left) half of complex plane. Approximation (31) would predict

$$R^{bb}[\omega(\boldsymbol{q})]-R^{aa}[\omega(\boldsymbol{q})]=m. \tag{34}$$

Indeed, we have checked that our numerical calculation of the residues satisfies (34) to an accuracy of 1.3%.

VII. FINAL REMARKS

In this paper we have studied the magnetic properties of the Hubbard model in honeycomb layers. Our study focused on the instabilities of the paramagnetic phase, on the magnetic phase diagram and on the collective excitations of the half-filled phase. Of particular interest is the fact that it is not possible to describe a true spiraling state in the honeycomb lattice, as opposed to the usual cubic case. As a consequence, the magnetic spiral order follows a kind of one dimensional path over the 2D lattice. This kind of ordering, here studied at mean field level, may have important consequences to the study of spin charge separation in 2D lattices. Also interesting, was the identification of two types of ferromagnetic order, which have eluded previous studies. For moderate values of U and electron densities not far from the half filled case, a region of weak ferromagnetism was found to have lower energy than the more usual Nagaoka ferromagnetic phase. The renormalization effect of the spin wave excitations on the Hartree-Fock magnetization was also studied. However, our calculation does not take into account the renormalization of the mean field critical U. It is well known that quantum fluctuations should induce an increase the value of U_c. Our calculation cannot capture this effect, since it only takes into account the effect of well defined spin waves. We believe, however, that the calculation can be extended to include the effect of high-energy damped particle-hole processes leading to a renormalization of U_c, but this would require a modification of our numerical calculations and a significant increase of the computational time.

APPENDIX A: USEFUL EXPRESSIONS FOR THE U_c CRITICAL LINES AT $q=0$

In this appendix, we derive the equations for the critical lines from the static susceptibilities ($\boldsymbol{q}=\mathbf{0}$ and $\omega=0$). Our

starting point is the zero order spin-spin susceptibility in Eq. (21) . The Green's functions in the paramagnetic region are obtained from Eqs. (12)–(15) after setting the magnetization to zero. Performing the Matsubara summations in Eq. (21), the analytical continuation and taking the zero frequency limit, we obtain

$$\chi^{(0)aa}_{+-,0}(\boldsymbol{q},0) = \frac{1}{4}\sum_{\boldsymbol{k}} [M_{++}(\boldsymbol{k},\boldsymbol{q}) + M_{+-}(\boldsymbol{k},\boldsymbol{q}) + M_{-+}(\boldsymbol{k},\boldsymbol{q}) + M_{--}(\boldsymbol{k},\boldsymbol{q})], \tag{A1}$$

$$\chi^{(0)ab}_{+-,0}(\boldsymbol{q},0) = \frac{1}{4}\sum_{\boldsymbol{k}} e^{i(\psi_{k-q}-\psi_k)}[M_{++}(\boldsymbol{k},\boldsymbol{q}) - M_{+-}(\boldsymbol{k},\boldsymbol{q}) - M_{-+}(\boldsymbol{k},\boldsymbol{q}) + M_{--}(\boldsymbol{k},\boldsymbol{q})], \tag{A2}$$

$$M_{\alpha,\beta}(\boldsymbol{k},\boldsymbol{q}) = \frac{\theta[E_\alpha(\boldsymbol{k})] - \theta[E_\beta(\boldsymbol{k}-\boldsymbol{q})]}{E_\alpha(\boldsymbol{k}) - E_\beta(\boldsymbol{k}-\boldsymbol{q})}, \tag{A3}$$

where $\psi_{\boldsymbol{k}}=\arg(\phi_{\boldsymbol{k}})$. The critical interaction strength, U_c, is given by $U_c/N=[\chi^{(0)aa}_{+-,0}\pm|\chi^{(0)ab}_{+-,0}|]^{-1}$, in the limit $\boldsymbol{q}\to\boldsymbol{0}$. Expanding all $\boldsymbol{q}$ dependent quantities around the point $\boldsymbol{q}=\boldsymbol{0}$ up to first order, we obtain

$$\chi^{(0)aa}_{+-,0}(\boldsymbol{q},0) = \frac{1}{4}\sum_{\boldsymbol{k}} \delta[(E_+(\boldsymbol{k})) + \delta(E_-(\boldsymbol{k}))] + \frac{\theta[|\phi_{\boldsymbol{k}}| - |D(\boldsymbol{k})|]}{|\phi_{\boldsymbol{k}}|} + \boldsymbol{q}\cdot(\cdots) + \cdots \tag{A4}$$

$$\chi^{(0)ab}_{+-,0}(\boldsymbol{q},0) = \frac{1}{4}\sum_{\boldsymbol{k}} \delta[(E_+(\boldsymbol{k})) + \delta(E_-(\boldsymbol{k}))] - \frac{\theta[|\phi_{\boldsymbol{k}}| - |D(\boldsymbol{k})|]}{|\phi_{\boldsymbol{k}}|} + \boldsymbol{q}\cdot(\cdots) + \cdots. \tag{A5}$$

Inserting this result in the expression for U_c gives (for $\boldsymbol{q}=0$):

$$\left(\frac{U_c}{N}\right)^{-1}_{+} = \frac{1}{2}\sum_{\boldsymbol{k}} \{\delta[E_+(\boldsymbol{k})] + \delta[E_-(\boldsymbol{k})]\}, \tag{A6}$$

$$\left(\frac{U_c}{N}\right)^{-1}_{-} = \frac{1}{2}\sum_{\boldsymbol{k}} \frac{\theta(|\phi_{\boldsymbol{k}}| - |D(\boldsymbol{k})|)}{|\phi_{\boldsymbol{k}}|}. \tag{A7}$$

We recognize the density of states, $\rho(\epsilon)=\frac{1}{N}\Sigma_{\boldsymbol{k}}\{\delta[E_+(\boldsymbol{k})+\mu-\epsilon]+\delta[E_-(\boldsymbol{k})+\mu-\epsilon]\}$, appearing in Eq. (A6), which is just the Stoner criterion. The critical interaction strengths are given by

$$U_{c,+} = \frac{2}{\rho(\mu)}, \tag{A8}$$

$$U_{c,-} = \frac{2}{\frac{1}{N}\sum_{\boldsymbol{k}} \frac{\theta(|\phi_{\boldsymbol{k}}|-|D(\boldsymbol{k})|)}{|\phi_{\boldsymbol{k}}|}}. \tag{A9}$$

Note that all t' and t'' dependence is contained in $D(\boldsymbol{k})$. Of course, these equations could also have been obtained by taking the limit $m_F, m_{\mathrm{AF}}\to 0$ in Eq. (27).

APPENDIX B: LARGE U RESULTS FOR THE SUSCEPTIBILITIES AND SPIN WAVES

We give asymptotic expressions for the susceptibilities $\chi^0_{+-}(z,\mathrm{q})$ and spin wave dispersion for a half-filled honeycomb antiferromagnetic layer with nearest neighbor hopping. In this case, the chemical potential $\mu=0$ and the two energy bands are given by $E(\mathrm{k})_\pm=\pm\sqrt{(Um/2)^2+|\phi_{\boldsymbol{k}}|^2}$.

The expressions for coherence factors appearing in the single electron propagators, expanded up to second order in t/U, are

$$|A_{\uparrow,+}(\mathbf{k})|^2 = |A_{\downarrow,-}(\mathbf{k})|^2 = |B_{\downarrow,+}(\mathbf{k})|^2 = |B_{\uparrow,-}(\mathbf{k})|^2 \approx \frac{|\phi(\mathbf{k})|^2}{U^2m^2}, \tag{B1}$$

$$|A_{\uparrow,-}(\mathbf{k})|^2 = |A_{\downarrow,+}(\mathbf{k})|^2 = |B_{\downarrow,-}(\mathbf{k})|^2 = |B_{\uparrow,+}(\mathbf{k})|^2 \approx 1 - \frac{|\phi(\mathbf{k})|^2}{U^2m^2}, \tag{B2}$$

$$A^*_{\downarrow,-}(\mathbf{k})B_{\downarrow,-}(\mathbf{k}) = -A^*_{\uparrow,+}(\mathbf{k})B_{\uparrow,+}(\mathbf{k}) = A^*_{\uparrow,-}(\mathbf{k})B_{\uparrow,-}(\mathbf{k}) = -A^*_{\downarrow,+}(\mathbf{k})B_{\downarrow,+}(\mathbf{k}) \approx \frac{\phi^*(\mathbf{k})}{Um}. \tag{B3}$$

We therefore may use the approximate expressions for the χ^0_{+-} susceptibilities.

$$\chi^{(0)aa}(z,\mathbf{q}) \approx -\frac{1}{N}\sum_{\mathbf{k}} \frac{1}{z - E(\mathbf{k}) - E(\mathbf{k}+\mathbf{q})} \times\left[1 - \frac{|\phi(\mathbf{k})|^2 + |\phi(\mathbf{k}+\mathbf{q})|^2}{U^2m^2}\right], \tag{B4}$$

$$\chi^{(0)bb}(z,\mathbf{q}) \approx \frac{1}{N}\sum_{\mathbf{k}} \frac{1}{z + E(\mathbf{k}) + E(\mathbf{k}+\mathbf{q})} \times\left[1 - \frac{|\phi(\mathbf{k})|^2 + |\phi(\mathbf{k}+\mathbf{q})|^2}{U^2m^2}\right], \tag{B5}$$

$$\chi^{(0)ba}(z,\mathbf{q}) \approx \frac{1}{N}\sum_{\mathbf{k}} \left[\frac{1}{z - E(\mathbf{k}) - E(\mathbf{k}+\mathbf{q})} - \frac{1}{z + E(\mathbf{k}) + E(\mathbf{k}+\mathbf{q})}\right]\frac{\phi(\mathbf{k})\phi^*(\mathbf{k}+\mathbf{q})}{U^2m^2}, \tag{B6}$$

$$\chi^{(0)ab}(z,\mathbf{q}) \approx \frac{1}{N}\sum_{\mathbf{k}} \left[\frac{1}{z - E(\mathbf{k}) - E(\mathbf{k}+\mathbf{q})} - \frac{1}{z + E(\mathbf{k}) + E(\mathbf{k}+\mathbf{q})}\right]\frac{\phi^*(\mathbf{k})\phi(\mathbf{k}+\mathbf{q})}{U^2m^2}. \tag{B7}$$

We anticipate that the spin wave energies are of order $z\approx t^2/U$ so that we may use the expansion

$$\frac{1}{z+E(\mathbf{k})+E(\mathbf{k}+\mathbf{q})} \approx \frac{1}{Um}\left[1-\frac{z}{Um}-\frac{|\phi(\mathbf{k})|^2+|\phi(\mathbf{k}+\mathbf{q})|^2}{U^2m^2}+\cdots\right]$$

in Eqs. (B4)–(B7). The condition (23) for the spin wave dispersion now takes the form

$$\frac{z^2}{U^2m^4}=\left\{1-\frac{1}{m}+\frac{4}{U^2m^3N}\left[\sum_{\mathbf{p}}|\phi(\mathbf{p})|^2\right]\right\}^2 - \frac{4}{U^2m^6}\left|\frac{1}{N}\sum_{\mathbf{p}}\phi^*(\mathbf{p})\phi(\mathbf{p}+\mathbf{q})\right|^2. \tag{B8}$$

But we must take into account that the self-consistent equation for the Hartree-Fock magnetization, expanded to second order in t/U, is

$$1-\frac{1}{m}\approx-\frac{2}{U^2m^3N}\left[\sum_{\mathbf{p}}|\phi(\mathbf{p})|^2\right] \tag{B9}$$

Introducing Eqs. (B9) and (B8) we finally obtain the spin wave dispersion

$$z=\omega(\mathbf{q}) \approx \frac{2}{Um}\sqrt{\left[\frac{1}{N}\sum_{\mathbf{p}}|\phi(\mathbf{p})|^2\right]^2-\left|\frac{1}{N}\sum_{\mathbf{p}}\phi^*(\mathbf{p})\phi(\mathbf{p}+\mathbf{q})\right|^2}, \tag{B10}$$

which agrees with the result predicted by the Holstein-Primakoff theory.

APPENDIX C: HOLSTEIN-PRIMAKOFF ANALYSIS OF THE HEISENBERG MODEL

The Heisenberg Hamiltonian in the honeycomb lattice is given by

$$H=\frac{J}{2}\sum_{i\in A,\boldsymbol{\delta}}\left[S_i^zS_{i+\boldsymbol{\delta}}^z+\frac{1}{2}(S_i^+S_{i+\boldsymbol{\delta}}^-+S_i^-S_{i+\boldsymbol{\delta}}^+)\right] + \frac{J}{2}\sum_{i\in B,\boldsymbol{\delta}}\left[\tilde{S}_i^z\tilde{S}_{i+\boldsymbol{\delta}}^z+\frac{1}{2}(\tilde{S}_i^+\tilde{S}_{i+\boldsymbol{\delta}}^-+\tilde{S}_i^-\tilde{S}_{i+\boldsymbol{\delta}}^+)\right]. \tag{C1}$$

We introduce two sets of operators

$$S_i^z=-a_i^\dagger a_i+S,\quad S_i^+=\sqrt{2S-a_i^\dagger a_i}\,a_i,\quad S_i^+=a_i^\dagger\sqrt{2S-a_i^\dagger a_i}, \tag{C2}$$

and

$$\tilde{S}_i^z=-b_i^\dagger b_i+S,\quad \tilde{S}_i^+=\sqrt{2S-b_i^\dagger b_i}\,b_i,\quad \tilde{S}_i^+=b_i^\dagger\sqrt{2S-b_i^\dagger b_i}. \tag{C3}$$

Making the usual linear expansion and introducing the momentum representation for the bosonic operators, the Hamiltonian can be written as

$$H=-JN_AzS^2+JzS\sum_{\boldsymbol{k}}(a_{\boldsymbol{k}}^\dagger a_{\boldsymbol{k}}+b_{\boldsymbol{k}}^\dagger b_{\boldsymbol{k}})+JS\sum_{\boldsymbol{k}}(\phi(\boldsymbol{k})a_{\boldsymbol{k}}b_{-\boldsymbol{k}} + \phi^*(\boldsymbol{k})b_{-\boldsymbol{k}}^\dagger a_{\boldsymbol{k}}^\dagger). \tag{C4}$$

Next we introduce a set of quasiparticle operators defined by

$$a_{\boldsymbol{k}}^\dagger=u_{\boldsymbol{k}}\gamma_{1,\boldsymbol{k}}^\dagger-v_{\boldsymbol{k}}^*\gamma_{2,\boldsymbol{k}},\quad b_{-\boldsymbol{k}}^\dagger=u_{\boldsymbol{k}}\gamma_{2,\boldsymbol{k}}^\dagger-v_{\boldsymbol{k}}^*\gamma_{1,\boldsymbol{k}}, \tag{C5}$$

where the coherence factors obey $|u_{\boldsymbol{k}}|^2-|v_{\boldsymbol{k}}|^2=1$. After introducing transformations (5) in the Hamiltonian we find

$$H=-JN_AzS^2+\sum_{\boldsymbol{k}}[2JzS|v_{\boldsymbol{k}}|^2-JS\phi(\boldsymbol{k})v_{\boldsymbol{k}}u_{\boldsymbol{k}}^*-JS\phi^*(\boldsymbol{k})v_{\boldsymbol{k}}^*u_{\boldsymbol{k}}] + \sum_{\boldsymbol{k};i=1,2}[JzS(|u_{\boldsymbol{k}}|^2+|v_{\boldsymbol{k}}|^2)-JS\phi(\boldsymbol{k})v_{\boldsymbol{k}}u_{\boldsymbol{k}}^* - JS\phi^*(\boldsymbol{k})v_{\boldsymbol{k}}^*u_{\boldsymbol{k}}]\gamma_{i,\boldsymbol{k}}^\dagger\gamma_{i,\boldsymbol{k}}+\sum_{\boldsymbol{k}}\{[-2JzSv_{\boldsymbol{k}}u_{\boldsymbol{k}}+JS\phi(\boldsymbol{k})v_{\boldsymbol{k}}v_{\boldsymbol{k}} + JS\phi^*(\boldsymbol{k})u_{\boldsymbol{k}}u_{\boldsymbol{k}}]\gamma_{1,\boldsymbol{k}}^\dagger\gamma_{2,\boldsymbol{k}}^\dagger+\text{H.c.}\}, \tag{C6}$$

which implies the conditions

$$JzS[(|u_{\boldsymbol{k}}|^2+|v_{\boldsymbol{k}}|^2)-JS\phi(\boldsymbol{k})v_{\boldsymbol{k}}u_{\boldsymbol{k}}^*-JS\phi^*(\boldsymbol{k})v_{\boldsymbol{k}}^*u_{\boldsymbol{k}}]=\omega(\boldsymbol{k}),$$
$$-2JzSv_{\boldsymbol{k}}u_{\boldsymbol{k}}+JS\phi(\boldsymbol{k})v_{\boldsymbol{k}}v_{\boldsymbol{k}}+JS\phi^*(\boldsymbol{k})u_{\boldsymbol{k}}u_{\boldsymbol{k}}=0. \tag{C7}$$

The second condition reveals that we can choose $u_{\boldsymbol{k}}$ to be real and $v_{\boldsymbol{k}}^*=\phi(\boldsymbol{k})\alpha(\boldsymbol{k})$, with $\alpha(\boldsymbol{k})$ real. After some straightforward manipulations we find

$$\omega(\boldsymbol{k})=JS\sqrt{z^2-|\phi_{\boldsymbol{k}}|^2},\quad \alpha^2(\boldsymbol{k})=-\frac{1}{2|\phi_{\boldsymbol{k}}|^2}+\frac{z}{2|\phi_{\boldsymbol{k}}|^2}\frac{JS}{\omega(\boldsymbol{k})}. \tag{C8}$$

The staggered magnetization is given by

$$m=S-\frac{1}{2N_A}\sum_{\boldsymbol{k}}\langle a_{\boldsymbol{k}}^\dagger a_{\boldsymbol{k}}+b_{\boldsymbol{k}}^\dagger b_{\boldsymbol{k}}\rangle =S-\frac{1}{N_A}\sum_{\boldsymbol{k}}\left(-\frac{1}{2}+\frac{1}{2}\frac{z}{\sqrt{z^2-|\phi_{\boldsymbol{k}}|^2}}\right) - \frac{1}{N_A}\sum_{\boldsymbol{k}}\frac{zn_B[\omega(\boldsymbol{k})]}{\sqrt{z^2-|\phi_{\boldsymbol{k}}|^2}}, \tag{C9}$$

and at zero temperature we assume $n_B[\omega(\boldsymbol{k})]=0$. Computing the integral gives a magnetization value of 0.24, that is about 50% the Néel value $\frac{1}{2}$.

[1] P. W. Anderson, Science **235**, 1196 (1987).
[2] L. Balents, M. P. A. Fisher, and S. M. Girvin, Phys. Rev. B **65**, 224412 (2002).
[3] K. Takada, H. Dakurai, E. Takayama-Muromachi, F. Izumi, R. A. Dilinian, and T. Sasaki, Nature (London) **422**, 53 (2003).
[4] K. Kuroki and R. Arita, Phys. Rev. B **63**, 174507 (2001).
[5] S. Onari, K. Kuroki, R. Arita, and H. Aoki, Phys. Rev. B **65**, 184525 (2002).
[6] See Tôru Moriya, Acta Phys. Pol. B **34**, 287 (2003); cond-mat/0207669 for a recent review on spin fluctuations and superconductivity.
[7] J. Nagamatsu, N. Nakagawa, T. Muranaka, Y. Zenitani, and J. Akimitsu, Nature (London) **410**, 63 (2001).
[8] J. Gonzalez, F. Guinea, and M. A. H. Vozmediano, Nucl. Phys. B **424**, 595 (1994); J. Gonzalez, F. Guinea, and M. A. H. Vozmediano, Phys. Rev. Lett. **77**, 3589 (1996).
[9] S. Sorella and E. Tosatti, Europhys. Lett. **19**, 699 (1992).
[10] L. M. Martelo, M. Dzierzawa, L. Siffert, and D. Baeriswyl, Z. Phys. B: Condens. Matter **103**, 335 (1997).
[11] N. Furukawa, J. Phys. Soc. Jpn. **70**, 1483 (2001).
[12] T. Hanisch, B. Kleine, A. Ritzl, and E. Müller-Hartmann, Ann. Phys. (N.Y.) **4**, 303 (1995).
[13] A. L. Tchougreeff and R. Hoffmann, J. Phys. Chem. **96**, 8933 (1992).
[14] G. Baskaran and S. A. Jafari, Phys. Rev. Lett. **89**, 016402 (2002).
[15] N. M. R. Peres, M. A. N. Arajo, and A. H. C. Neto, Phys. Rev. Lett. **92**, 199701 (2004); G. Baskaran, and S. A. Jafari, *ibid.* **92**, 199702 (2004).
[16] N. M. R. Peres and M. A. N. Araújo, Phys. Rev. B **65**, 132404 (2002).
[17] N. M. R. Peres and M. A. N. Araújo, Phys. Status Solidi **236**, 523 (2003).
[18] H. R. Krishnamurthy, C. Jayaprakash, S. Sarker, and W. Wenzel, Phys. Rev. Lett. **64**, 950 (1990).
[19] A. P. Kampf, Phys. Rev. B **53**, 747 (1996).
[20] More general spin states, as those discussed by Subir Sachdev in Rev. Mod. Phys. **75**, 913 (2003), are outside the scope of our treatment. However, the states we consider in this paper are included in the analysis of the earlier reference.
[21] J. Burgy, M. Mayr, V. Martin-Mayor, A. Moreo, and E. Dagotto, Phys. Rev. Lett. **87**, 277202 (2001).
[22] A. Singh and Z. Tesanovic, Phys. Rev. B **41**, 11 457 (1990); **41**, 11 604 (1990); **45**, 7258 (1992).
[23] The calculations presented in this figure were performed at the GCEP cluster, in the Center of Physics of the University of Minho.